ORIGINAL ARTICLE

Effects of Number of Lenses in Microlens Arrays on Field of View in Integral Imaging Systems

Pei-Chuen Chiou and Jia-Han Li*

Department of Engineering Science and Ocean Engineering, National Taiwan University, Taiwan

(**Received** 25 January 2014; **Accepted** 11 March 2014; **Published on line** 1 June 2015)

*Corresponding author email: jiahan@ntu.edu.tw

DOI: 10.5875/ausmt.v5i2.552

Abstract: In integral imaging, the microlens array (MLA) is the key element for capturing 3D information. The microlens array can be used to encode light originating from different directions into the photosensor, producing images called elemental images. By extracting and rearranging the pixels in each elemental image, one can obtain images from different view angles, known as sub-images. Elemental images can also be used for depth reconstruction. This paper computationally reconstructs the object planes of different depths, using a blocking mask to investigate the effects of the number of lenses in the microlens array on the field of view. It is found that the MLA field of view increases with the number of lenses, but the resolution of the resulting sub-images can be improved by increasing the amount of light information captured by each lens.

Keywords: Microlens Array; Integral Imaging; Elemental Image; Depth Reconstruction

Introduction

Early in 1908, Lippmann proposed a concept called an integral photograph [1] which can record light rays and then optically or computationally reconstruct a 3D scene. Today, three-dimensional sensing and visualization applications capture 3D information using microlens arrays (MLA) which have several advantages including small size, light weight, and ease of mass production. In integral imaging, the microlens array sorts light rays according to their direction or origin, and then encodes them in the photosensor, thus allowing for depth reconstruction. Thus, microlens arrays are widely used in various applications, such as 3D sensing [2, 3], 3D displays [4, 5], 3D reconstruction [6-9], 3D underwater imaging [10, 11], and medical imaging [12, 13]. Using MLAs in light field cameras for integral imaging allows for the capture of both the directional light field but also the depth of field information. Conventional cameras only record the intensity of light rays and thus lose all directional information. By using the MLA, light rays from elemental images can be captured and their 3D information can be used for depth reconstruction. One reconstruction method is to computationally map elemental images pixel-to-pixel into the desired depth [14].

We introduce an experimental setup to capture the elemental images of real scenes. The captured data is then processed according to sub-image theory to produce images from different perspectives. A separate case using an MLA with fewer microlenses is conducted to compare the resulting image fields of views. Computational integral imaging reconstruction is used to reconstruct image depth using elemental images.

Principles

Integral imaging

Figure 1 demonstrates the concept of integral imaging. The principle can be explained through geometric optics. In the pickup process, light reflected by objects is captured by the MLA and recorded by the camera to produce an elemental image. This 3D information is then projected back to the same MLA. Figure 1 shows a 5x5 MLA demonstration purposes, and the figure is not drawn to scale.

Figure 2 illustrates the acquisition of the field of

view and depth information by MLA. The light rays reflected by the object can be sorted by the MLA according to different depths or field of views. The camera records elemental images, which contain information for the object from different directions.

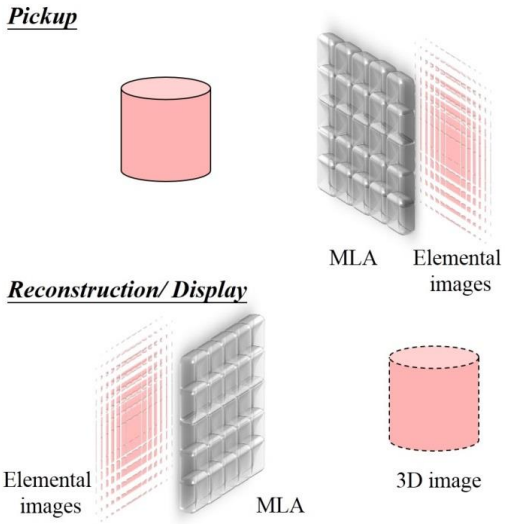

Figure 1. Principle of integral imaging for pickup and reconstruction.

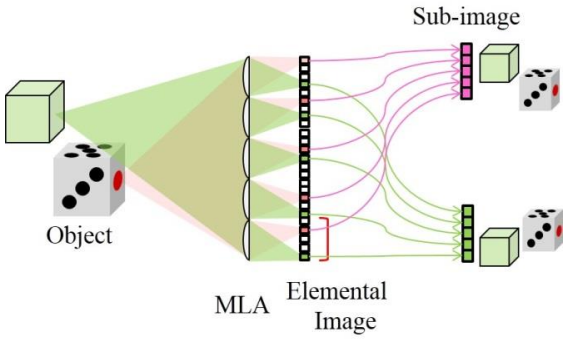

Figure 2. MLA capturing field of view and depth information.

Digitally rearranging the locations of specific pixels of each elemental image produces sub-images from different perspectives, as shown in Figure 3. The sub-images reveal distinct separations, and thus contain depth data. Let E_{kl} be the k-th row and l-th column elemental image, then the pixel value at coordinate (k, l) in the sub-image can be expressed as (1), where I_{mn} is the m-th row and the n-th column of the sub-image in the sub-image array:

$$I_{mn}(k,l) = E_{kl}(m,n). \quad (1)$$

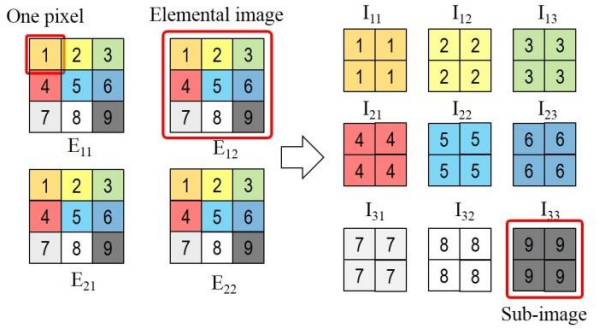

Figure 3. Formation of sub-images from elemental images.

Computational integral imaging reconstruction

As previously mentioned, the elemental images can store field of view and depth information of real scenes. The multi-perspective property of these 2D images can be used to computationally reconstruct a particular field of view or depth plane. As shown in Figure 4, in a computational volumetric reconstruction, the magnified elemental images are mapped pixel-to-pixel and overlapped with other projected elemental images on the reconstruction plane using a computer-synthesized virtual pinhole array [15]. Assume z is the distance between the virtual pinhole array and the reconstructed plane and g is the distance between the pinhole array and the elemental image array; the magnification M of each overlapped elemental image can thus be calculated by $M=z/g$. To simplify the expression, Figure 4 presents a one-dimensional analysis, and the extension to a two-dimensional real case analysis is straightforward. The object plane of different depths can be reconstructed accordingly.

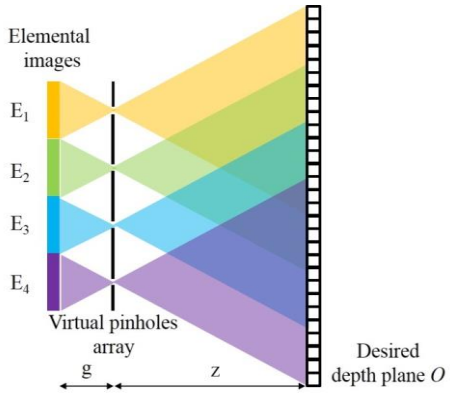

Figure 4. The principle of computational volumetric reconstruction with a virtual pinhole array.

Experimental Results and Discussion

This section presents two experimental setup cases. One case places a mask in front of the MLA to reduce the number of microlenses, while the other does not use a mask. The effect of the number of microlenses on field of

Pei-Chuen Chiou is an M.S. candidate in the Department of Engineering Science and Ocean Engineering at National Taiwan University, Taiwan. Her main field of research is light field optics.

Jia-Han Li received his Ph.D. in electrical and computer engineering from Purdue University in 2005, where he studied nanophotonics, including near-field irregular diffractive optical element and plasmonic field enhancements. He joined Department of Engineering Science and Ocean Engineering in National Taiwan University in 2006. His current research interests include nanolithography, plasmonics, metamaterials, terahertz devices, solar photonics, near field optics, biophotonics, scientific computation, and optical engineering. He is a member of IEEE, OSA, and APS.

view is discussed.

Experimental setup

Figure 5(a) illustrates the pickup process, where the objects are set at 60 mm, 96 mm, and 130 mm from the camera, that is, the die 1 plane is conjugated with the elemental image plane. As shown in Figute 5(b), a mask is placed in front of the MLA to reduce the number of microlenses. The mask is used as a pupil to block some light rays going through the MLA. The size of the mask is 10 mm × 10 mm, while the square hollowed in the center is 3.75 mm × 3.75 mm. The hollowed area contains a 25 × 25 microlens array, and the pitch between microlenses is 0.15 mm. The three objects are illuminated by incoherent light, and these objects are used as the 3D objects in the experiment. Figure 6 shows a photo of the experimental setup.

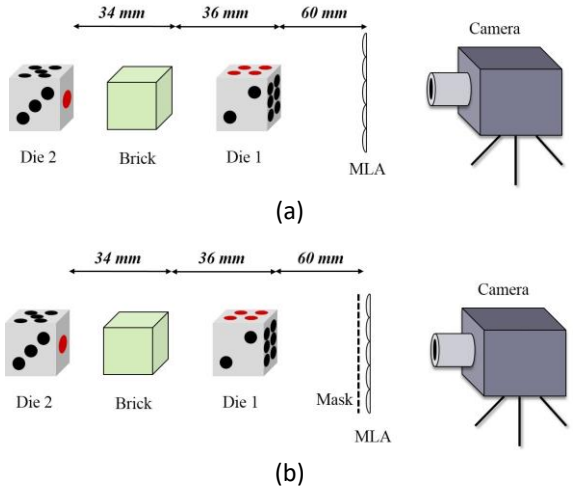

Figure 5. Illustrations of experimental setup, where (a) is the case without a mask and (b) is the case with a mask.

The MLA used in the experiment has 66 × 66 round refractive lenses each with a diameter of 0.146 mm and a pitch of 0.15 mm. The focal length of each microlens is 6.7 mm, so the calculated f number is 6.7 mm/0.146mm = 45.9. A USB microscope is used to capture the images.

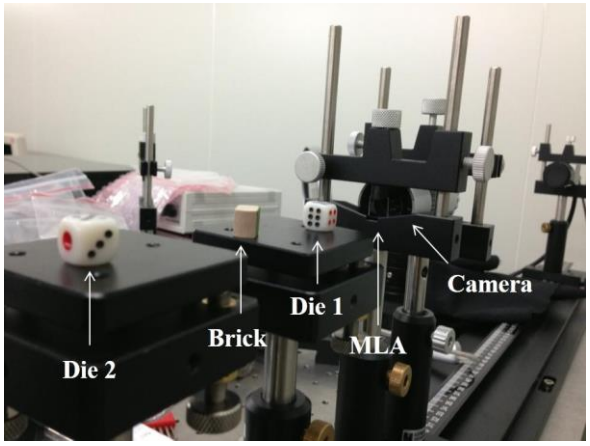

Figure 6. Experimental setup for pickup stage.

Measurement results

Figure 7(a) shows the elemental image array with 66 × 66 element images captured in our pickup system without a mask; the size of each elemental image is 16 pixels × 16 pixels. When the mask is used, there are 25 × 25 elemental images each measuring 16 × 16 pixels in the same CCD zoom-in rate, as shown in Figure 7(b). Furthermore, not all pixels in the CCD are used in this experiment because we have cropped the original captured image to remove the area of the lens mount.

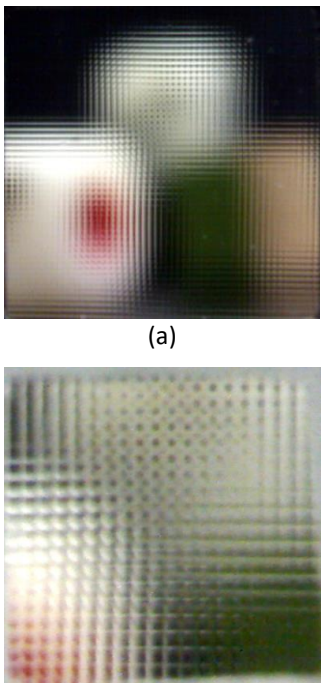

Figure 7. Captured elemental image array, where (a) is without a mask and (b) is with a mask.

As illustrated in Figure 3, we extracted the pixels at same location of each elemental image and relocated them according to their corresponding position in an elemental image. The corresponding sub-image arrays as shown in Figure 8(a) have 16 × 16 images and the size of each sub-image is 66 × 66 pixels. As we can see in Figure 8(b), the array has 16 × 16 sub-images each measuring 25 × 25 pixels, but no single sub-image can show even a part of real scene due to the low number of microlens in the pickup system. The 25 × 25 microlens array collected only 625 elemental images each measuring 16 × 16 pixels. Therefore, each sub-image is merely composed of 256 pixels. Moreover, the 25 × 25 microlens array is only able to record a small part of the light rays coming from different directions. That is, the directional information is not sufficient to construct images of the real scene. Comparing Figures 8(a) and 8(b) shows that the field of

view of a MLA with the blocked mask is smaller than that of a full MLA.

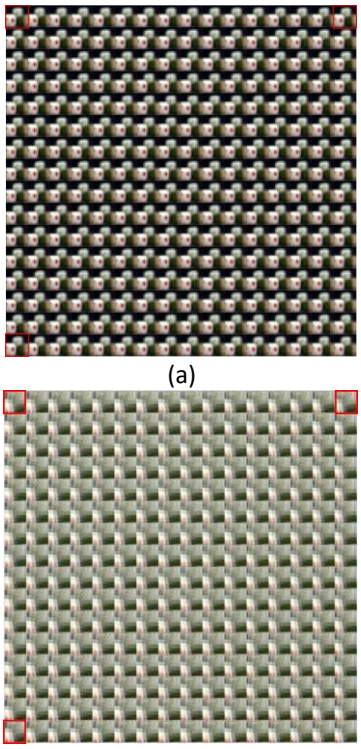

Figure 8. Corresponding sub-image array extracted from the element image array shown in Figure 7(a) is for the case without a mask, and (b) is the case with a mask.

The different fields of view in these sub-images produce parallax shifts between them. To show the horizontal and vertical parallax shifts clearly, the differences between red-marked images are calculated for each case, as shown in Figure 9. The vertical parallax shift is calculated by subtracting the top left and bottom left sub-images in the sub-image array, as shown in Figure 8, and the horizontal one is calculated by subtracting the top left and upper right sub-images. The sub-images are magnified for clarity.

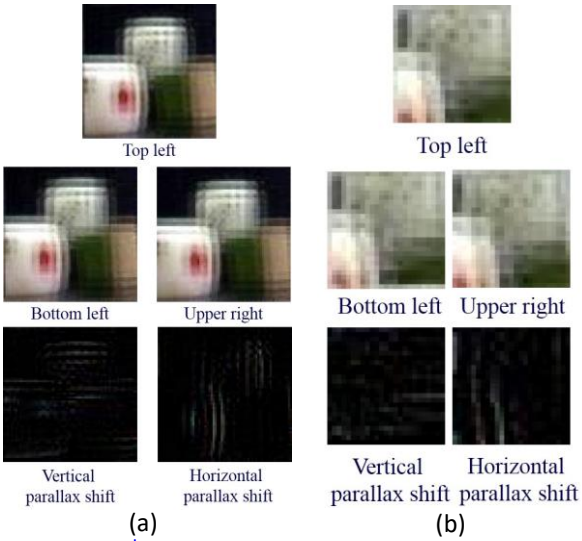

Figure 9. Magnification of red-marked sub-images in Figure 8 and their corresponding parallax shifts between sub-images. (a) is for the case without a mask, and (b) is the case with a mask.

3D computational reconstruction

The object planes of different depths can be computed by the computational volumetric reconstruction method, shown in Figure 4. The elemental image used for depth reconstruction is as shown in Figure 8.

Figure 10 shows the reconstructed images of different depths using a computer-synthesized virtual pinhole array. The left and right images respectively show the three objects without a mask and with a mask. However, the reconstruction results are not obvious, due to the large *f/#* of the MLA in the pickup stage resulting in insufficient depth information. Furthermore, the size of each elemental image is only 16 × 16 pixels, which is inadequate to compute high quality reconstructed images.

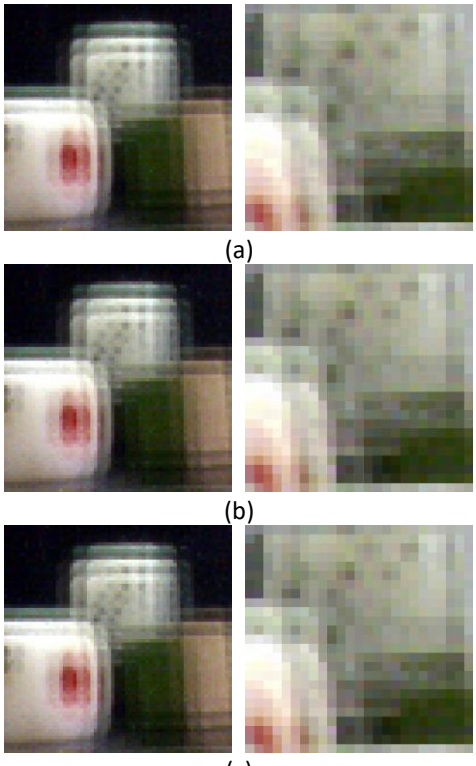

Figure 10. Reconstructed images focusing on (a) die 1 (b) the brick and (c) die 2 for the cases without a mask (on the left column) and with a mask (on the right column).

Conclusion

An experimental setup is demonstrated to pick up 3D information from objects in 2D elemental images. The pixels in these images are then digitally extracted and relocated to obtain sub-images. The parallax shifts are also demonstrated. This method can be useful for the quick

production of sub-images. These multi-perspective 2D images were then used to demonstrate the field of view for the object planes. For 3D reconstruction, object planes with different depths are also reconstructed using computational volumetric reconstruction. By inserting an aperture between the objects and the microlens array (MLA), the depth of the reconstructed images can be more distinctly ascribed to the smaller *f/#* of the MLA. It is also found that the field of view (FOV) of the pickup system increases with the number of microlenses in the MLA, due to each microlens capturing light coming from more directions. By controlling the resolution in each element image taken from each lens of the microlens array, the resolution of the corresponding sub-image can be increased. This setup also allows for evaluation of the effect of the number of lenses in the microlens array on depth information of the reconstructed images. Such assessments can be useful for the further optimization of microlens arrays with various lens sizes.

Acknowledgment

Support from the Ministry of Science and Technology of Taiwan through 102-2221-E-002-006 and 102-2221-E-002-005 is gratefully acknowledged.

References

[1] M. G. Lippmann, "Épreuves réversibles donnant la sensation du relief," *Journal of Theoretical and Applied PhysicS,* vol. 7, no. 1, pp. 821-825, 1908. doi: 10.1051/jphystap:019080070082100

[2] S. Kishk and B. Javidi, "Improved resolution 3d object sensing and recognition using time multiplexed computational integral imaging," *Opt Express,* vol. 11, no. 26, pp. 3528-3541, 2003. doi: 10.1364/OE.11.003528

[3] A. Stern and B. Javidi, "Three-dimensional image sensing, visualization, and processing using integral imaging," *Proceedings of the IEEE,* vol. 94, no. 3, pp. 591-607, 2006. doi: 10.1109/JPROC.2006.870696

[4] H. Navarro, R. Martinez-Cuenca, G. Saavedra, M. Martinez-Corral, and B. Javidi, "3d integral imaging display by smart pseudoscopic-to-orthoscopic conversion (spoc)," *Opt Express,* vol. 18, no. 25, pp. 25573-25583, 2010. doi: 10.1364/oe.18.025573

[5] M. A. Alam, M.-L. Piao, G. Li, Y. Piao, and N. Kim, "Three dimensional projection-type integral imaging display system using directional projection and elemental image resizing method," in proceeding of *InforInternational Conference on matics, Electronics & Vision (ICIEV)*, Dhaka, Bangladesh, May 17-18, 2013, pp. 1-4. doi: 10.1109/ICIEV.2013.6572619

[6] D.-H. Shin and E.-S. Kim, "Computational integral imaging reconstruction of 3d object using a depth conversion technique," *Journal of the Optical Society of Korea,* vol. 12, no. 3, pp. 131-135, 2008. doi: 10.3807/JOSK.2008.12.3.131

[7] D.-H. Shin, D.-J. Kim, and B.-G. Lee, "Computational integral imaging reconstruction method of 3-d images based on pixel-to-pixel mapping and interpolation technique," in proceeding of Digital Holography and Three-Dimensional Imaging 2009, Vancouver, Canada, April 26-30, 2009. doi: 10.1364/DH.2009.DWB18

[8] M. Cho, and B. Javidi, "Computational reconstruction of three-dimensional integral imaging by rearrangement of elemental image pixels," *Journal of Display Technology, ,* vol. 5, no. 2, pp. 61-65, 2009. doi: 10.1109/JDT.2008.2004857

[9] G. Li, S.-C. Kim, and E.-S. Kim, "Viewing quality-enhanced reconstruction of 3-d object images by using a modified computational integral- imaging reconstruction technique," *3D Research,* vol. 3, no. 3, pp. 1-9, 2012. doi: 10.1007/3DRes.03(2012)4

[10] R. Schulein and B. Javidi, "Underwater multi-view three-dimensional imaging," *Journal of Display Technology,* vol. 4, no. 4, pp. 351-353, 2009. doi: 10.1109/JDT.2008.924161

[11] A. Kanaev and W. Hou "Restoration of turbulence degraded underwater images," *Optical Engineering,* vol. 84, no. 8, p. 057007, 2012. doi: 10.1117/2.1201211.004542

[12] M. Levoy, R. Ng, A. Adams, M. Footer, and M. Horowitz, "Light field microscopy," *ACM Transactiion on Graph.,* vol. 25, no. 3, pp. 924-934, 2006. doi: 10.1145/1141911.1141976

[13] Y.-T. Lim, J.-H. Park, K.-C. Kwon, and N. Kim, "Resolution-enhanced integral imaging microscopy that uses lens array shifting," *Optics Express,* vol. 17, no. 21, pp. 19253-19263, 2009. doi: 10.1364/oe.17.019253

[14] D.-H. Shin and H. Yoo, "Scale-variant magnification for computational integral imaging and its application to 3d object correlator," *Optics Express,* vol. 16, no. 12, pp. 8855-8867, 2008. doi: 10.1364/OE.16.008855